Cell Reports

Identification of a discrete subpopulation of spinal cord ependymal cells with neural stem cell properties

Graphical abstract

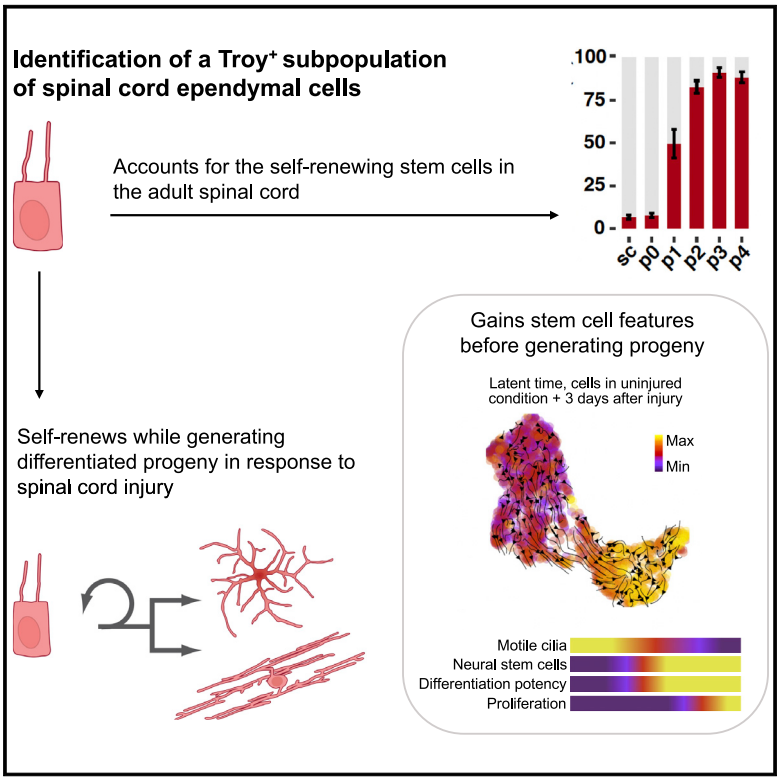

Highlights

- Troy expression defines a subpopulation of spinal cord ependymal (EpA) cells
- EpA cells harbor the *in vitro* stem cell capacity of the adult spinal cord
- EpA cells dedifferentiate and acquire stem cell properties after spinal cord injury
- EpA cells self-renew while generating astrocytes and oligodendrocytes after injury

Authors

Moa Stenudd, Hanna Sabelström, Enric Llorens-Bobadilla, ..., Christian Göritz, Fanie Barnabé-Heider, Jonas Frisén

Correspondence

jonas.frisen@ki.se

In brief

Stenudd et al. identify a subpopulation of ependymal cells defined by Troy expression, EpA cells, that contains the *in vitro* stem cell capacity of the spinal cord. These cells dedifferentiate to self-renewing stem cells after spinal cord injury and generate scar-forming astrocytes as well as oligodendrocytes.

Stenudd et al., 2022, Cell Reports *38*, 110440
March 1, 2022
https://doi.org/10.1016/j.celrep.2022.110440

Cell Reports

CellPress
OPEN ACCESS

Report

Identification of a discrete subpopulation of spinal cord ependymal cells with neural stem cell properties

Moa Stenudd,[1] Hanna Sabelström,[1] Enric Llorens-Bobadilla,[1] Margherita Zamboni,[1] Hans Blom,[2] Hjalmar Brismar,[2] Shupei Zhang,[1] Onur Basak,[3,4] Hans Clevers,[3,4] Christian Göritz,[1,5] Fanie Barnabé-Heider,[1,6] and Jonas Frisén[1,7,*]

[1]Department of Cell and Molecular Biology, Karolinska Institutet, 171 77 Stockholm, Sweden
[2]Science for Life Laboratory, Department of Applied Physics, Royal Institute of Technology, 171 21 Solna, Sweden
[3]Hubrecht Institute for Developmental Biology and Stem Cell Research, 3584 CT Utrecht, the Netherlands
[4]University Medical Centre Utrecht, 3584 GC, Utrecht, the Netherlands
[5]Ming Wai Lau Centre for Reparative Medicine, Stockholm Node, Karolinska Institutet, 171 77 Stockholm, Sweden
[6]Department of Neuroscience, Karolinska Institutet, 171 77 Stockholm, Sweden
[7]Lead contact
*Correspondence: jonas.frisen@ki.se
https://doi.org/10.1016/j.celrep.2022.110440

SUMMARY

Spinal cord ependymal cells display neural stem cell properties *in vitro* and generate scar-forming astrocytes and remyelinating oligodendrocytes after injury. We report that ependymal cells are functionally heterogeneous and identify a small subpopulation (8% of ependymal cells and 0.1% of all cells in a spinal cord segment), which we denote ependymal A (EpA) cells, that accounts for the *in vitro* stem cell potential in the adult spinal cord. After spinal cord injury, EpA cells undergo self-renewing cell division as they give rise to differentiated progeny. Single-cell transcriptome analysis revealed a loss of ependymal cell gene expression programs as EpA cells gained signaling entropy and dedifferentiated to a stem-cell-like transcriptional state after an injury. We conclude that EpA cells are highly differentiated cells that can revert to a stem cell state and constitute a therapeutic target for spinal cord repair.

INTRODUCTION

Ependymal cells lining the central canal of the spinal cord do not generate other cell types under physiological conditions. However, the ependymal cell population harbors cells with *in vitro* neural stem cell properties in the adult spinal cord, and after a lesion, they produce the majority of new astrocytes forming the glial scar as well as some remyelinating oligodendrocytes (Barnabé-Heider et al., 2010; Beattie et al., 1997; Cusimano et al., 2018; Johansson et al., 1999; Lacroix et al., 2014; Li et al., 2016, 2018; Meletis et al., 2008; Mothe and Tator, 2005; North et al., 2015; Pfenninger et al., 2011). Ependymal cell-derived astrocytes limit tissue damage and further severance of axons and are a source of neurotrophic factors supporting the survival of neurons in the injured spinal cord (Sabelström et al., 2013). Reduction of the ependymal cell contribution to scar formation impairs spontaneous functional recovery (Cusimano et al., 2018; North et al., 2015). In contrast, promotion of oligodendrocyte generation from ependymal cells after injury increases remyelination and promotes recovery of axon conductance (Llorens-Bobadilla et al., 2020), demonstrating that influencing the response of ependymal cells to injury holds therapeutic potential.

There is heterogeneity in morphology and marker expression of spinal cord ependymal cells, and a first indication that there is also functional heterogeneity was demonstrated by isolation of a subpopulation with enriched neurosphere initiation capacity (Fiorelli et al., 2013; Sabourin et al., 2009). However, these neurospheres did not self-renew efficiently, and it was not established whether this subpopulation gives rise to progeny after injury, leaving open the key question of the identity of the cells harboring stem cell potential and generating progeny after spinal cord injury.

RESULTS

Characterization of a subpopulation of spinal cord ependymal cells with *in vitro* neural stem cell properties

We used genetic fate mapping in transgenic mice with cell type-specific expression of tamoxifen-inducible Cre recombinase (CreER) on a Rosa26 reporter background to assess functional heterogeneity among ependymal cells in the adult spinal cord. A small subset (8.2% ± 1.2%, mean ± SEM) of ependymal cells, which we denote ependymal A (EpA) cells, was recombined in the adult spinal cord of Troy-CreER knockin mice (Figure S1A; Stange et al., 2013). Troy (*Tnfrsf19*) is a tumor necrosis factor receptor family member expressed by stem cells; for example, in the adult forebrain and in the gastrointestinal tract (Basak et al., 2018; Fafilek et al., 2013; Stange et al., 2013). In

addition to this subpopulation of ependymal cells, sparse fibroblast-like cells/pericytes and endothelial cells were recombined (Figure S1B). We found *Tnfrsf19* transcripts in 44 (86%) of 51 EpA cells analyzed using RNAscope, with an average of 2.1 (±0.08) transcripts detected per EpA cell (Figure S1C).

EpA cells were most abundant in the dorsal pole of the ependymal layer (Figures 1A and 1B). Spinal cord ependymal cells are morphologically heterogeneous (Bruni and Reddy, 1987; Meletis et al., 2008), and super-resolution microscopy revealed that EpA cells had a basal process that often contacted a blood vessel (Figure 1A). EpA cells uniformly expressed the pan-ependymal cell markers FoxJ1, Sox2, Sox9, and Vimentin (Figures 1C and S1D–S1F), whereas only a small subset expressed Nestin (Figure S1G and S1H). Troy-CreER recombined EpA cells appeared as highly differentiated cells and proliferated at the same low rate as the overall ependymal cell population (Figures S1I and S1J).

Neural stem cells can be propagated *in vitro* from ependymal cells in the adult spinal cord (Barnabé-Heider et al., 2010; Johansson et al., 1999; Meletis et al., 2008; Pfenninger et al., 2011). We induced recombination in Troy-CreER mice and generated neurospheres after a 1-week tamoxifen-clearing period (Barnabé-Heider et al., 2010; Meletis et al., 2008). In primary neurosphere cultures, we found a similar recombination rate as in ependymal cells from the same mice ($p = 0.59$, Student's t test; Figures 1D and 1E), not indicating any enrichment of primary neurosphere-forming potential in the EpA population. However, the recombination rate increased when the neurosphere cultures were passaged. From the second passage, the vast majority of neurospheres from Troy-CreER mice were recombined and, hence, derived from EpA cells (Figures 1E and S2A). This is in contrast to what was seen for a previously described ependymal cell subpopulation that was enriched for primary neurosphere formation potential but lacked efficient self-renewal capacity (Fiorelli et al., 2013; Sabourin et al., 2009). Thus, many primary neurospheres derive from ependymal cells with limited self-renewal capacity, and the cultures are taken over by long-term neural stem cells over time. Because recombination is seldom complete, the high proportion of recombined neurospheres after repeated passages suggests that Troy-CreER recombined EpA ependymal cells account for all, or close to all, cells with extensive *in vitro* self-renewal capacity in the adult spinal cord. EpA cell-derived neurospheres generated astrocytes, neurons, and oligodendrocytes when exposed to differentiating conditions *in vitro* (Figures S2B–S2D) and, thus, display neural stem cell properties.

EpA cells give rise to astrocytes and oligodendrocytes after spinal cord injury

To assess the response of EpA cells to injury, recombination was induced, and mice were subjected to a lesion after a 1-week tamoxifen-clearing period. Troy-CreER recombined EpA ependymal cells generated migrating progeny 1 week after a dorsal *funiculus* incision or a crush lesion (Figures 2A–2C). The population of recombined ependymal and ependymally derived cells expanded approximately 5-fold after injury (Figure 2D). Recombined astrocytes and oligodendrocytes were found 15 weeks after injury (Figures 2E–2G). We never saw recombined ependymal cell-derived neurons *in vivo*.

Blood vessel-associated cells proliferate in response to spinal cord injury, but only the progeny of type A pericytes leave the vessel wall as they differentiate to fibroblast-like cells, and perivascular cells do not give rise to astrocytes or oligodendrocytes (Göritz et al., 2011). Troy-CreER recombined blood vessel-associated cells were not found to generate progeny that left the vessel wall following injury (Figure S3A).

Almost all EpA ependymal cells expressed the neural stem cell-associated protein Nestin after injury (Figures S3B and S3C). The number of EpA cells in the ependymal layer remained stable after injury, suggesting that they self-renew to maintain the population while producing migrating progeny (Figure 2B).

We next wanted to determine whether Troy-CreER expression marks a transient ependymal cell state or cells with stable features over time. We administered tamoxifen to induce recombination and then waited 1 week, 2 months, or 15 months before making an injury. This resulted in a comparable extent and distribution of recombined ependymal cell progeny (Figure S3D), suggesting that Troy-CreER recombination does not mark a transient cell state different ependymal cells take on at different times but that it marks cells with stable properties.

Clonal analysis of the response of EpA ependymal cells to spinal cord injury

To further examine the injury response by EpA cells, we conducted a clonal analysis. Troy-CreER mice on an R26-confetti reporter background (Snippert et al., 2010) received tamoxifen to induce low, stochastic recombination (Figure S4A). After a 2-week tamoxifen-clearing period, the mice were subjected to dorsal *funiculus* incisions (Figure S4B). We analyzed the spinal cords 2 weeks later. We observed a low recombination rate with, on average, one ependymal cell expressing a specific reporter gene every 400 μm to 11 mm, enabling identification of individual clones with high confidence (Figures S4C and S4D).

We identified 20 Troy-CreER recombined clones in 12 animals containing EpA ependymal cell progeny that had incorporated 5-ethynyl-2'-deoxyuridine (EdU) and left the ependymal layer after the spinal cord injury (Figure 3A). For half of the EpA-derived clones, no vessel-associated cell recombined to express the same color as the clone was found within the same or neighboring sections.

One-third of all EpA ependymal cells residing within the injured segment had generated migrating Sox2-expressing progeny (Figure S4E). All EpA cells that had generated migrating progeny were located in the dorsal or lateral ependymal layer, and we did not find any clone with migrating cells generated from a ventrally located EpA cell (Figures S4F and S4G). Some ependymal cell progeny migrated dorsally and/or laterally to a location distant from the ependymal layer, whereas there was much less spread along the rostrocaudal axis (Figures 3B and 3C). Each clone contained 1–6 migrating cells, with the largest clones being close to or rostral to the injury epicenter (Figure 3D).

We identified an ependymal cell with the same fluorescent reporter within 100 μm rostral or caudal to the migrating cell(s) for 17 of 20 clones (Figure S4H). In the three cases where we did not find an ependymal cell expressing the same reporter nearby, the reason may be technical; in two cases, a tissue section close to the migrating cell was lost during processing; in one case, the

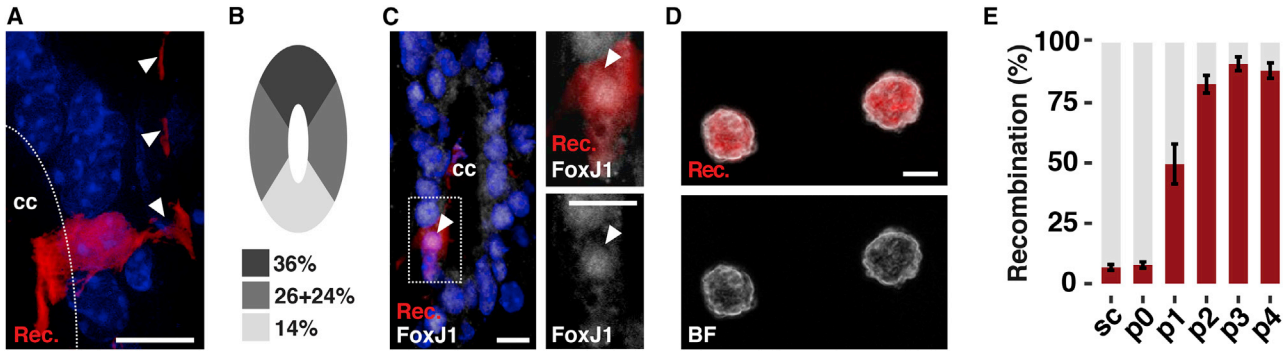

Figure 1. A subpopulation of spinal cord ependymal cells harbors the *in vitro* neural stem potential of the adult spinal cord

(A) A Troy-CreER recombined EpA ependymal cell with a basal process (arrowheads).

(B) Distribution of EpA cells in the ependymal layer.

(C) A recombined EpA cell (arrowhead) expressing FoxJ1.

(D and E) EpA cells generate neurospheres (D) that self-renew efficiently (E).

(A) shows a 12-μm-thick section, and (C) shows a 2-μm confocal plane. Scale bars, 10 μm (A and C) and 50 μm (D). Error bars represent SEM. Cell nuclei are visualized with DAPI and appear blue. Rec, recombined; cc, central canal; p, passage.

tissue was distorted by the injury, and the ependymal layer was difficult to delineate. There were 5 clones that contained one ependymal cell and a single migrating daughter cell. In addition to the clones consisting of ependymal and migrating cells, we found 7 clones of clustered ependymal cells expressing the same reporter without associated migrating progeny. There were 10 clones containing one or several ependymal cells and migrating progeny (Figure S4I). The identification of a nearby ependymal founder cell indicates that individual ependymal cells can generate migrating progeny without being consumed in the process, demonstrating self-renewal capacity at the single-cell level *in vivo*.

EpA cells acquire a stem-cell-like transcriptional state after injury

The finding that highly differentiated EpA cells self-renew and give rise to astrocytes and oligodendrocytes after injury prompted us to explore the molecular underpinnings of this process using droplet-based single-cell RNA sequencing. We induced recombination, and after a 2-week tamoxifen-clearing period, one group of mice was subjected to a dorsal *funiculus* incision lesion. Three days later, we isolated recombined cells by flow cytometry from the injured spinal cord and from the corresponding region of uninjured spinal cord (Figure S5A). The isolated sample contained ependymal cells, vessel-associated cells, and a couple of other contaminating populations (Figures S5B–S5F; STAR Methods).

We performed dimensionality reduction with uniform manifold approximation and projection (UMAP), followed by trajectory analysis with Monocle 3 on the whole dataset. EpA cells clustered separately, with separate trajectories, from all other cell types in the sample (Figures S5G and S5H). When repeating the analysis on a dataset containing only endothelial cells and pericytes, we saw a clear separation between the endothelial cell and pericyte lineages (Figure S6A). Among endothelial cells, only cells from injured spinal cord tend to be present later in the trajectory, suggesting an injury reaction (Figure S6).

For our EpA cell population, we performed dimensionality reduction with principal-component analysis (PCA) followed by UMAP using the 20 top principal components and 2,000 highly variable genes as input. We identified three adjacent clusters. The EpA1 cluster contained cells from the injured and uninjured spinal cords, whereas the EpA2 and EpA3 clusters consisted almost exclusively of cells from the injured spinal cord (Figures 4A, 4B, and S7A). Approximately 41% of the recombined EpA cells from the injured spinal cords clustered with cells from uninjured spinal cords in EpA1, suggesting that these cells did not mount a response to the injury, potentially because of their location at a distance from the lesion (5-mm-long pieces of injured spinal cord were used for the analysis).

We constructed single-cell trajectories using RNA velocity and Monocle 3 (Bergen et al., 2020; Cao et al., 2019), two different methods that place cells along latent time/pseudotime corresponding to the progression of each cell in a process. Latent time (RNA velocity) and pseudotime (Monocle 3) scores placed EpA1 cells first in the trajectory, followed by EpA2 and then EpA3 (Figures 4C and S7B). As expected by their quiescence, RNA velocity using a dynamic model revealed vector fields (seen as arrows) with little directionality in resting EpA1 cells. However, as cells transitioned to EpA2-EpA3 during their activation after injury, velocity fields gained directionality toward EpA3 (Figure 4C).

Cells in the EpA1 cell cluster expressed the highest levels of genes associated with motile cilia and other differentiated ependymal cell markers, including, for example, *Foxj1*, *Fam183b*, *Rarres2*, and *Tmem212*, which were expressed at lower levels or not at all in EpA2 and EpA3 cells (Figure S7C). *Tnfrsf19* (Troy) expression was higher in the EpA1 and EpA2 cluster compared with the EpA3 cluster (Figure S7D). *Tnfrsf19* expression was detected in ~20% of EpA cells in uninjured and injured animals in this analysis, which is an expected share because of large transcript dropout rates when detecting lowly expressed genes such as *Tnfrsf19* (Figure S1C) with droplet-based sequencing methods (Svensson et al., 2017). Cells in

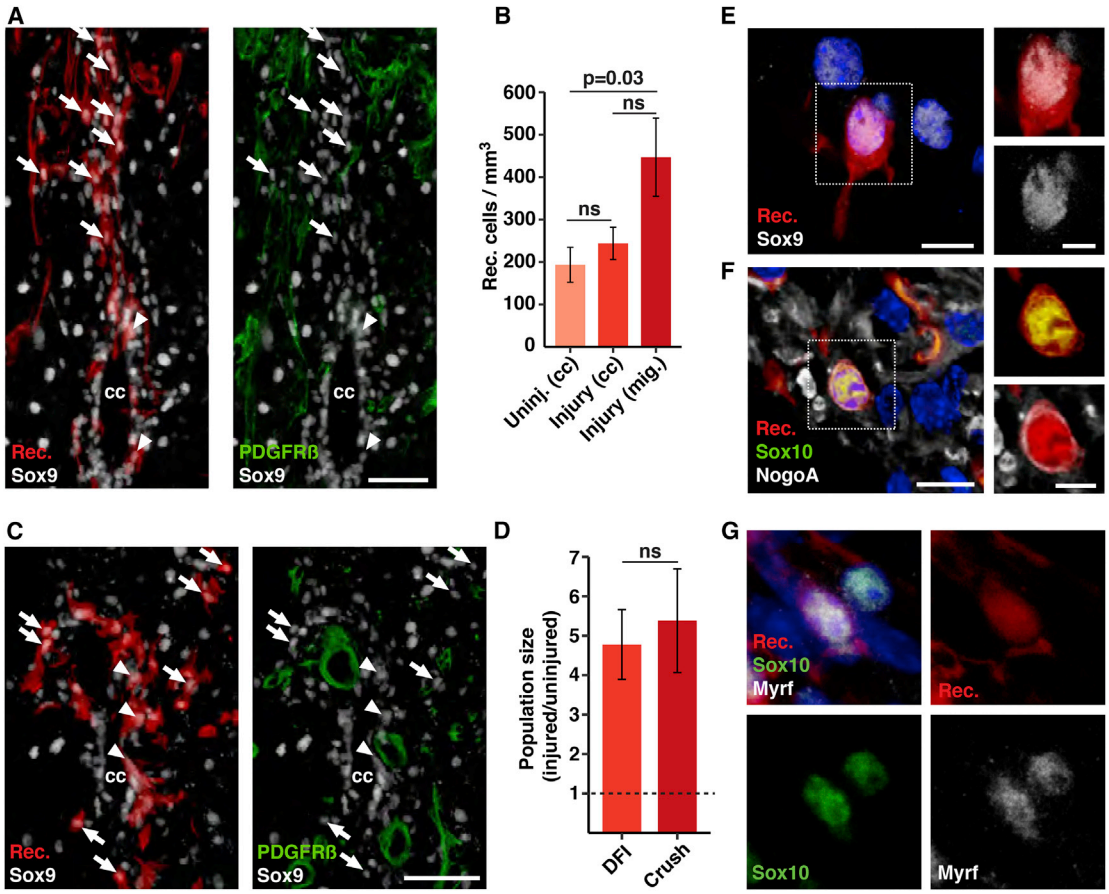

Figure 2. EpA cells give rise to astrocytes and oligodendrocytes after spinal cord injury

(A) EpA ependymal cells (arrowheads) generate migrating progeny positive for the astrocyte marker Sox9 and negative for the stromal cell marker platelet-derived growth factor receptor beta (PDGFRβ) (arrows) in response to a dorsal *funiculus* incision injury.

(B) The number of EpA ependymal cells is maintained after a dorsal *funiculus* incision, indicating that they self-renew to maintain their population while generating migrating progeny.

(C) EpA cells (arrowheads) generate migrating Sox9+/PDGFRβ− progeny (arrows) after a spinal cord crush injury.

(D) EpA population size after dorsal *funiculus* and crush injury, normalized to EpA population size in uninjured spinal cord.

(E–G) Recombined Sox9-expressing astrocytes (E), a recombined Sox10/NogoA expressing oligodendrocyte (F), and a recombined Sox10/Myrf-expressing oligodendrocyte (G) in the dorsal *funiculus* in the same injury site 15 weeks after injury.

Scale bars: 25 μm (A), 50 μm (B and D), 10 μm (left panels of F and G), and 5 μm (right panels of F and G). The p values are from one-way ANOVA followed by Tukey's post hoc test. Error bars represent SEM. Cell nuclei are visualized with DAPI and appear blue. Rec, recombined; Uninj, uninjured; mig, migrating; DFI, dorsal *funiculus* incision.

the EpA2 cluster had higher expression of ribosomal and translation-related genes, and cells in the EpA3 cluster, in addition, expressed cell cycle genes (Figure 4E). The number of expressed genes increased gradually from EpA1 to EpA3, whereas the proportion of mitochondrial genes had the opposite progression, from highest in EpA1 to lowest in EpA3 cells (Figure S7E).

The differentiation potential of single cells can be estimated by analysis of the interconnectedness of signaling networks in RNA sequencing data, resulting in a signaling entropy score (Teschendorff and Enver, 2017). Signaling entropy increased with pseudotime and was highest in the EpA3 cluster (Figures 4F and S7F). The increased signaling entropy coincided with a gradual increase in the number of unique genes expressed in each cell (Figure S7G), which may allow the cells to activate diverse differentiation programs. Indeed, at this point, there was an increase in expression of genes relating to cell differentiation, migration, and proliferation (Figures S7H–S7K) and, more specifically, genes associated with the astrocyte and oligodendrocyte lineages (Figures 4G and 4H).

To better understand the transcriptional changes between the EpA clusters (and along pseudotime), we identified active gene regulatory networks using SCENIC (single-cell regulatory network inference and clustering) (Aibar et al., 2018). We then used AUCell to determine the regulon activity in each cell. Also looking at gene regulatory network activity, we found higher ependymal cell-related regulon activity in EpA1 cells, with, for instance, high Rfx2 and Rfx3 activity (Zeisel et al., 2015;

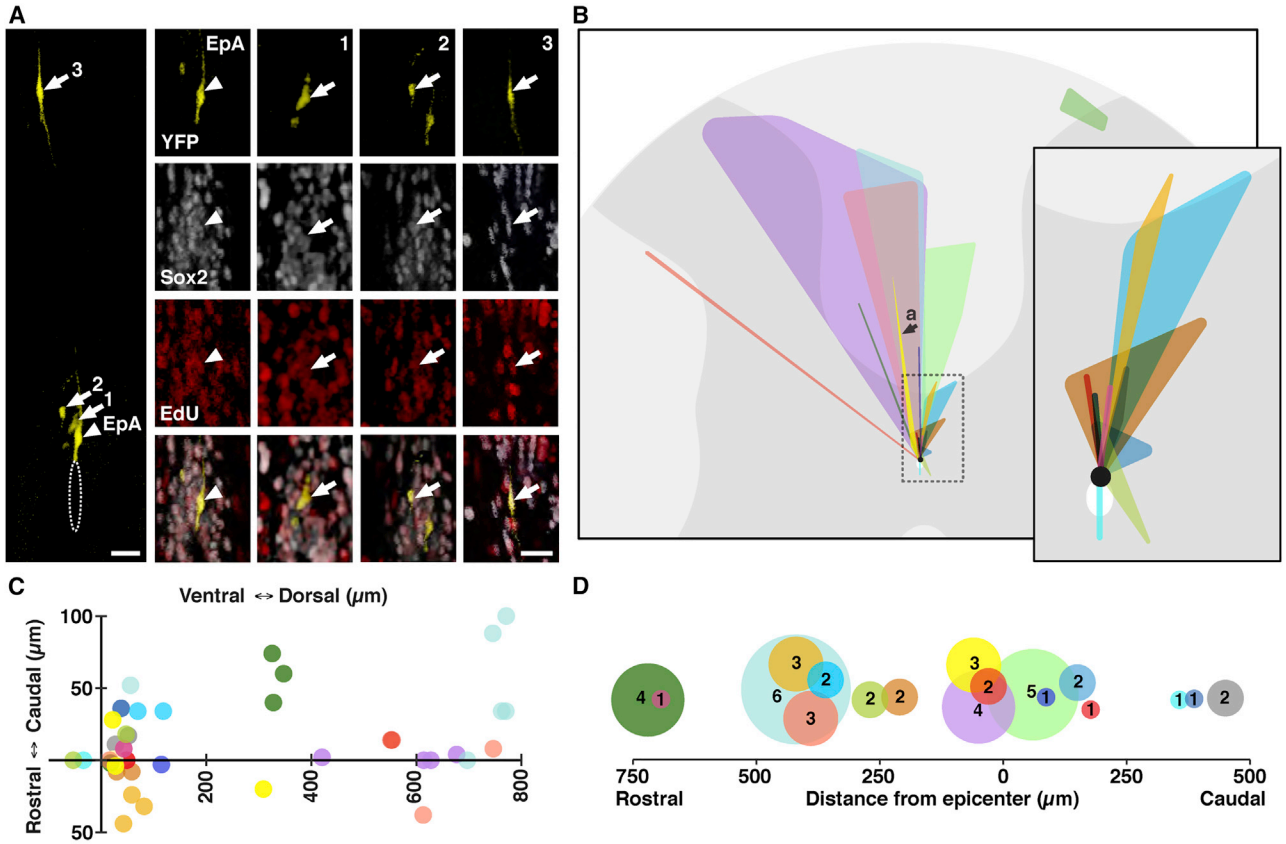

Figure 3. Clonal analysis of the response of EpA ependymal cells to spinal cord injury

(A) A Troy-CreER recombined YFP-expressing clone 2 weeks after a dorsal *funiculus* injury, containing one EpA cell and three migrated progeny (1–3), which express Sox2 and have incorporated EdU.

(B) Illustration of the distribution of clones containing migrated cells. The inset shows a magnification of the area within the dashed line with short-migrated clones only.

(C) Migrated progeny from EpA ependymal cells display a limited spread along the rostrocaudal axis, whereas they often migrate greater distances within the lesioned area in the dorsal portion of the spinal cord. Origo represents the location of the founder cell.

(D) Number of migrated progeny per clone in relation to the distance from the injury epicenter.

Each clone is represented by the same unique color. The YFP clone in (A) is yellow in (B)–(D). Scale bars, 25 μm.

Figure S7L). In the EpA2 cluster, we detected high activity of stem cell-, differentiation-, and neurogenesis-associated regulons, such as Sox4, Sox11, Tead2, and Gata3 (Kizil et al., 2012; Miao et al., 2019; Mu et al., 2012; Tamm et al., 2011; Figure S7M). In the EpA3 cluster, we found regulon activity for proliferation- and neurogenesis-related genes, such as the polymerase subunit gene Pole3 as well as Brca1 and Ezh2 (Hakem et al., 1996; Hwang et al., 2014; Figure S7N).

A comparison of the gene expression signature of cells in the subventricular zone neural stem cell lineage with EpA cells demonstrated increased expression of stem cell signature genes in EpA2 and EpA3 and of transit-amplifying signature genes in EpA3 cells (Figures 4I and 4J; Tables S3 and S4). The observation also held when cell cycle genes were excluded from the analysis. This unfolding of a stem-cell-like transcriptional state is likely to underlie the self-renewal capacity and multipotency EpA cells exhibit after spinal cord injury.

DISCUSSION

We report identification of a subpopulation of spinal cord ependymal cells that self-renews efficiently and gives rise to neurons, astrocytes, and oligodendrocytes *in vitro*. EpA cells acquire a stem-cell-like transcriptional state and undergo self-renewing divisions as they give rise to differentiated progeny after spinal cord injury. This identifies EpA cells as stem cells of the adult spinal cord.

We show that EpA cells express genes typical for highly differentiated ependymal cells, such as motile cilium genes. Expression of genes marking the differentiated ependymal state decreases rapidly after spinal cord injury; the cells gain signaling entropy (a proxy marker for multilineage potential) become more similar to subventricular zone transit-amplifying and stem cells and enter the cell cycle. Thus, rather than directly differentiating to astrocyte- or oligodendrocyte-lineage cells, EpA cells dedifferentiate to acquire a stem-cell-like state. This may be a

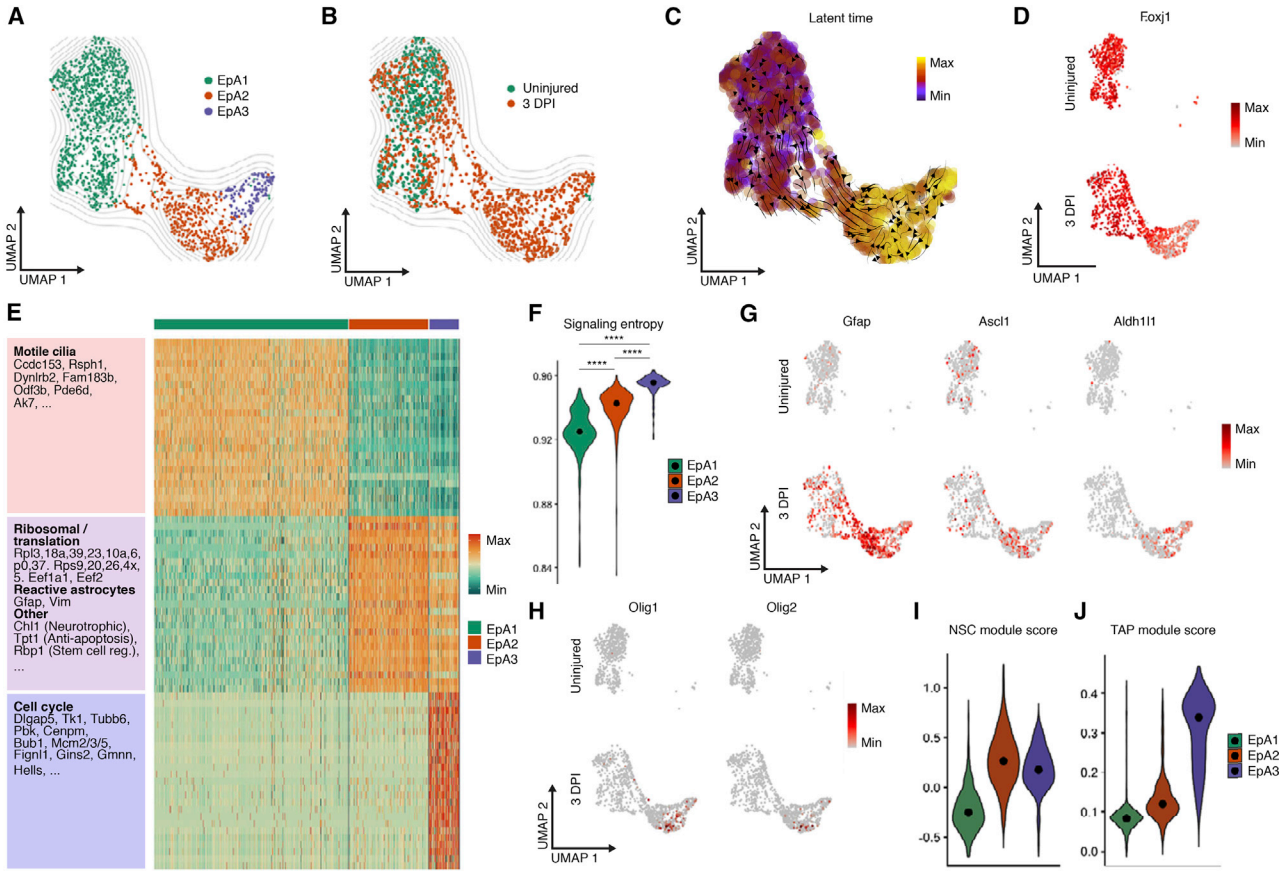

Figure 4. Single-cell RNA sequencing (scRNA-seq) reveals EpA cells gaining stem cell features after injury

(A) UMAP projection of Troy-CreER Rec EpA cells without injury and 3 days after a DFI, colored by cluster.

(B) UMAP projection of EpA cells, colored by condition.

(C) UMAP colored by latent time progression. Cells later in the trajectory (determined by RNA velocity) are yellow. The UMAP is overlaid by arrows showing extrapolated future states of cells, suggesting a trajectory in the direction from the EpA1 cluster toward the EpA3 cluster.

(D) UMAP projection colored by expression of the motile cilium gene Foxj1.

(E) Heatmap of the top 25 differentially expressed genes per cluster (Tables S1 and S2).

(F) Signaling entropy is a proxy marker for differentiation potency, and it is increased in EpA progeny clusters formed after spinal cord injury.

(G) UMAP projection with EpA cells and their progeny colored by expression of genes expressed in astrocytes. Ascl1 is relatively evenly distributed between the clusters. Gfap expression increases in the EpA2 cluster and stays high in the EpA3 cluster. Aldh1l1 is highest in the EpA3 cluster.

(H) UMAP projection with EpA cells and their progeny colored by expression of the transcription factors Olig1 and Olig2.

(I and J) A comparison of the gene expression signature of cells in the subventricular zone neural stem cell lineage with EpA cells shows increased expression of neural stem cell signature genes in EpA2 and EpA3 and of transit-amplifying progenitor signature genes in EpA3 cells.

DPI, days post injury; Comp, component; reg, regulation; NSC, neural stem cell; TAP, transit-amplifying progenitor. The p values in (F) are from a Kruskal-Wallis test followed by Dunn's post hoc test. Black points in violin plots indicate the median.

prerequisite for EpA cells to self-renew and not be consumed by the process of generating progeny.

The transition of EpA cells from a highly differentiated ependymal cell state to a stem-cell-like state and their generation of other differentiated cells after injury is reminiscent of the process in which parenchymal astrocytes gives rise to new neurons after a stroke. After a striatal stroke, local astrocytes undergo similar transcriptional changes as we describe here for EpA cells to reach a stem-cell-like state before initiating neurogenesis (Magnusson et al., 2014, 2020). This latent stem cell potential of some differentiated glial cells appears to be evolutionarily conserved, but with a much more limited role in regeneration in the adult mammalian central nervous system. In lower vertebrates, differentiated glial cells drive much of the successful regeneration after central nervous system lesions, such as the complete spinal cord repair by ependymal cells or retinal regeneration by Müller glia (Becker et al., 2018; Hoang et al., 2020; Tazaki et al., 2017).

There is emerging evidence that the regenerative potential of glial cells in the adult mammalian central nervous system can be expanded. An understanding of the transcriptome of parenchymal astrocytes led to identification of synergistic effects of reduced Notch signaling, mitogens, and injury, allowing experimental expansion of striatal neurogenesis as well as recruitment of astrocytes to the neurogenic lineage in the cerebral cortex (Magnusson et al., 2020; Santopolo et al., 2020;

Zamboni et al., 2020). The discovery of chromatin accessibility for latent genetic differentiation programs in ependymal cells directed development of a strategy to massively increase generation of remyelinating oligodendrocytes, resulting in recovery of axon conductance after spinal cord injury (Llorens-Bobadilla et al., 2020). Identifying EpA cells, which constitute only ~0.1% of all cells in a spinal cord segment, as latent stem cells defines a target cell population for regenerative therapeutic interventions for spinal cord repair.

Limitations of the study

Although we demonstrate that single EpA cells give rise to neurospheres that generate neurons, astrocytes, and oligodendrocytes *in vitro* and that EpA cells, at the population level, give rise to astrocytes and oligodendrocytes after injury, we did not demonstrate multipotency at the single-cell level *in vivo*. To assess this, one would need to perform more extensive clonal analyses and wait longer after spinal cord injury because oligodendrocyte generation is rare and takes a long time. At this point, we do not understand how EpA cells differ at the molecular level from other spinal cord ependymal cells to endow them with the potential to take on stem cell properties *in vitro* and after spinal cord injury.

STAR★METHODS

Detailed methods are provided in the online version of this paper and include the following:

- KEY RESOURCES TABLE
- RESOURCE AVAILABILITY
  - Lead contact
  - Materials availability
  - Data and code availability
- EXPERIMENTAL MODEL AND SUBJECT DETAILS
  - Transgenic mice
- METHOD DETAILS
  - Genetic labeling of transgenic mice
  - Spinal cord injury
  - EdU labeling
  - Neural stem cell cultures
  - Immunohistochemistry
  - Immunocytochemistry
  - *In situ* hybridization with RNAscope
  - Microscopy
  - 3D structured illumination microscopy (3D-SIM)
  - Single cell RNA sequencing
- QUANTIFICATION AND STATISTICAL ANALYSIS
  - Uninjured tissue
  - Neurospheres
  - Injury site quantifications
  - Clonal analysis
  - Single cell RNA sequencing analysis

SUPPLEMENTAL INFORMATION

Supplemental information can be found online at https://doi.org/10.1016/j.celrep.2022.110440.

ACKNOWLEDGMENTS

We thank M. Djelloul and X. Li for discussions, J.E. Goldman for the O4 antibody, and M. Wegner for the Myrf antibody. This study was supported by grants from the Swedish Research Council, the Swedish Cancer Society, the Swedish Foundation for Strategic Research, Knut och Alice Wallenbergs Stiftelse, and the IRP Schellenberg Foundation. E.L.-B. was supported by an IRP Schellenberg Foundation postdoctoral fellowship.

AUTHOR CONTRIBUTIONS

M.S., H.S., and J.F. designed the study. M.S. and J.F. wrote the manuscript. M.S., H.S., E.-L.B., M.Z., and S.Z. conducted experiments. H. Blom and H. Brismar supervised super-resolution microscopy. O.B. and H.C. provided the Troy-CreER and Rosa26-confetti mouse lines. C.G., F.B.-H., and J.F. supervised the experiments.

DECLARATION OF INTERESTS

J.F., E.L.-B., and M.Z. are consultants to 10x Genomics.

Received: November 25, 2020
Revised: November 30, 2021
Accepted: February 3, 2022
Published: March 1, 2022

SUPPORTING CITATION

The following reference appears in the supplemental information: Vanlandewijck et al. (2018).

REFERENCES

Aibar, S., González-blas, C.B., Moerman, T., Huynh-thu, V.A., Imrichova, H., Hulselmans, G., Rambow, F., Marine, J., Geurts, P., Aerts, J., et al. (2018). Europe PMC funders group Europe PMC funders author manuscripts SCENIC: single-cell regulatory network inference and clustering. Nat. Methods *14*, 1083–1086.

Barnabé-Heider, F., Göritz, C., Sabelström, H., Takebayashi, H., Pfrieger, F.W., Meletis, K., and Frisén, J. (2010). Origin of new glial cells in intact and injured adult spinal cord. Cell Stem Cell *7*, 470–482.

Basak, O., Krieger, T.G., Muraro, M.J., Wiebrands, K., Stange, D.E., Frias-Aldeguer, J., Rivron, N.C., van de Wetering, M., van Es, J.H., van Oudenaarden, A., et al. (2018). Troy+ brain stem cells cycle through quiescence and regulate their number by sensing niche occupancy. Proc. Natl. Acad. Sci. *115*, E610–E619.

Beattie, M.S., Bresnahan, J.C., Komon, J., Tovar, C.A., Van Meter, M., Anderson, D.K., Faden, A.I., Hsu, C.Y., Noble, L.J., Salzman, S., et al. (1997). Endogenous repair after spinal cord contusion injuries in the rat. Exp. Neurol. *148*, 453–463.

Becker, C.G., Becker, T., and Hugnot, J.P. (2018). The spinal ependymal zone as a source of endogenous repair cells across vertebrates. Prog. Neurobiol. *170*, 67–80.

Bergen, V., Lange, M., Peidli, S., Wolf, F.A., and Theis, F.J. (2020). Generalizing RNA velocity to transient cell states through dynamical modeling. Nat. Biotechnol. *38*, 1408–1414.

Bruni, J.E., and Reddy, K. (1987). Ependyma of the central canal of the rat spinal cord: a light and transmission electron microscopic study. J. Anat. *152*, 55–70.

Cao, J., Spielmann, M., Qiu, X., Huang, X., Ibrahim, D.M., Hill, A.J., Zhang, F., Mundlos, S., Christiansen, L., Steemers, F.J., et al. (2019). The single-cell transcriptional landscape of mammalian organogenesis. Nature *566*, 496–502.

Cusimano, M., Brambilla, E., Capotondo, A., Feo, D. De, Tomasso, A., Comi, G., Adamo, P.D., Muzio, L., and Martino, G. (2018). Selective killing of spinal

cord neural stem cells impairs locomotor recovery in a mouse model of spinal cord injury. J. Neuroinflammation *15*, 1–14.

Durinck, S., Spellman, P.T., Birney, E., and Huber, W. (2009). Mapping identifiers for the integration of genomic datasets with the R/bioconductor package biomaRt. Nat. Protoc. *4*, 1184–1191.

Fafilek, B., Krausova, M., Vojtechova, M., Pospichalova, V., Tumova, L., Sloncova, E., Huranova, M., Stancikova, J., Hlavata, A., Svec, J., et al. (2013). Troy, a tumor necrosis factor receptor family member, interacts with lgr5 to inhibit wnt signaling in intestinal stem cells. Gastroenterology *144*, 381–391.

Fiorelli, R., Cebrian-Silla, A., Garcia-Verdugo, J.-M., and Raineteau, O. (2013). The adult spinal cord harbors a population of GFAP-positive progenitors with limited self-renewal potential. Glia *61*, 2100–2113.

Frisén, J., Fried, K., Sjögren, A.-M., and Risling, M. (1993). Growth of ascending spinal axons in CNS scar tissue. Int. J. Devl. Neurosci. *11*, 461–475.

Göritz, C., Dias, D.O., Tomilin, N., Barbacid, M., Shupliakov, O., and Frisen, J. (2011). A pericyte origin of spinal cord scar tissue. Science *333*, 238–242.

Gustafsson, M.G.L., Shao, L., Carlton, P.M., Wang, C.J.R., Golubovskaya, I.N., Cande, W.Z., Agard, D.A., and Sedat, J.W. (2008). Three-dimensional resolution doubling in wide-field fluorescence microscopy by structured illumination. Biophys. J. *94*, 4957–4970.

Hakem, R., De La Pompa, J.L., Sirard, C., Mo, R., Woo, M., Hakem, A., Wakeham, A., Potter, J., Reitmair, A., Billia, F., et al. (1996). The tumor suppressor gene Brca1 is required for embryonic cellular proliferation in the mouse. Cell *85*, 1009–1023.

Hoang, T., Wang, J., Boyd, P., Wang, F., Santiago, C., Jiang, L., Yoo, S., Lahne, M., Todd, L.J., Jia, M., et al. (2020). Gene regulatory networks controlling vertebrate retinal regeneration. Science *370*, eabb8598.

Hwang, W.W., Salinas, R.D., Siu, J.J., Kelley, K.W., Delgado, R.N., Paredes, M.F., Alvarez-Buylla, A., Oldham, M.C., and Lim, D.A. (2014). Distinct and separable roles for EZH2 in neurogenic astroglia. Elife *3*, 1–19.

Johansson, C.B., Momma, S., Clarke, D.L., Risling, M., Lendahl, U., and Frisén, J. (1999). Identification of a neural stem cell in the adult mammalian central nervous system. Cell *96*, 25–34.

Kizil, C., Kyritsis, N., Dudczig, S., Kroehne, V., Freudenreich, D., Kaslin, J., and Brand, M. (2012). Regenerative neurogenesis from neural progenitor cells requires injury-induced expression of Gata3. Dev. Cell *23*, 1230–1237.

Lacroix, S., Hamilton, L.K., Vaugeois, A., Beaudoin, S., Breault-Dugas, C., Pineau, I., Lévesque, S.A., Grégoire, C.A., and Fernandes, K.J.L. (2014). Central canal ependymal cells proliferate extensively in response to traumatic spinal cord injury but not demyelinating lesions. PLoS One *9*, e85916.

Li, X., Floriddia, E.M., Toskas, K., Fernandes, K.J.L., Guerout, N., and Barnabe-Heider, F. (2016). Regenerative potential of ependymal cells for spinal cord injuries over time. EBioMedicine *13*, 55–65.

Li, X., Floriddia, E.M., Toskas, K., Chalfouh, C., Honore, A., Aumont, A., Vallières, N., Lacroix, S., Fernandes, K.J.L., Guérout, N., et al. (2018). FoxJ1 regulates spinal cord development and is required for the maintenance of spinal cord stem cell potential. Exp. Cell Res. *368*, 84–100.

Liu, K., Lu, Y., Lee, J.K., Samara, R., Willenberg, R., Sears-Kraxberger, I., Tedeschi, A., Park, K.K., Jin, D., Cai, B., et al. (2010). PTEN deletion enhances the regenerative ability of adult corticospinal neurons. Nat. Neurosci. *13*, 1075–1081.

Llorens-Bobadilla, E., Chell, J.M., Le Merre, P., Wu, Y., Zamboni, M., Bergenstråhle, J., Stenudd, M., Sopova, E., Lundeberg, J., Shupliakov, O., et al. (2020). A latent lineage potential in resident neural stem cells enables spinal cord repair. Science *370*, eabb8795.

Magnusson, J., Göritz, C., Tatarishvili, J., Dias, D.O., Smith, E.M., Lindvall, O., Kokaia, Z., and Frisén, J. (2014). A latent neurogenic program in astrocytes regulated by Notch signaling in the mouse. Science *346*, 237–241.

Magnusson, J.P., Zamboni, M., Santopolo, G., Mold, J.E., Barrientos-Somarribas, M., Talavera-Lopez, C., Andersson, B., and Frisén, J. (2020). Activation of a neural stem cell transcriptional program in parenchymal astrocytes. Elife *9*, 1–25.

McInnes, L., Healy, J., Saul, N., and Großberger, L. (2018). UMAP: uniform manifold approximation and projection. J. Open Source Softw. *3*, 861.

Meletis, K., Barnabé-Heider, F., Carlén, M., Evergren, E., Tomilin, N., Shupliakov, O., and Frisén, J. (2008). Spinal cord injury reveals multilineage differentiation of ependymal cells. PLoS Biol. *6*, e182.

Miao, Q., Hill, M.C., Chen, F., Mo, Q., Ku, A.T., Ramos, C., Sock, E., Lefebvre, V., and Nguyen, H. (2019). SOX11 and SOX4 drive the reactivation of an embryonic gene program during murine wound repair. Nat. Commun. *10*, 1–20.

Mothe, A., and Tator, C. (2005). Proliferation, migration, and differentiation of endogenous ependymal region stem/progenitor cells following minimal spinal cord injury in the adult rat. J. Neurosci. *131*, 177–187.

Mu, L., Berti, L., Masserdotti, G., Covic, M., Michaelidis, T.M., Doberauer, K., Merz, K., Rehfeld, F., Haslinger, A., Wegner, M., et al. (2012). SoxC transcription factors are required for neuronal differentiation in adult hippocampal neurogenesis. J. Neurosci. *32*, 3067–3080.

North, H.A., Pan, L., McGuire, T.L., Brooker, S., and Kessler, J.A. (2015). 1-Integrin alters ependymal stem cell BMP receptor localization and attenuates astrogliosis after spinal cord injury. J. Neurosci. *35*, 3725–3733.

Pfenninger, C.V., Steinhoff, C., Hertwig, F., and Nuber, U.A. (2011). Prospectively isolated CD133/CD24-positive ependymal cells from the adult spinal cord and lateral ventricle wall differ in their long-term in vitro self-renewal and in vivo gene expression. Glia *59*, 68–81.

Sabelström, H., Stenudd, M., Réu, P., Dias, D.O., Elfineh, M., Zdunek, S., Damberg, P., Göritz, C., and Frisén, J. (2013). Resident neural stem cells restrict tissue damage and neuronal loss after spinal cord injury in mice. Science *342*, 637–640.

Sabourin, J.C., Ackema, K.B., Ohayon, D., Guichet, P.O., Perrin, F.E., Garces, A., Ripoll, C., Charité, J., Simonneau, L., Kettenmann, H., et al. (2009). A mesenchymal-like ZEB1+ niche harbors dorsal radial glial fibrillary acidic protein-positive stem cells in the spinal cord. Stem Cells *27*, 2722–2733.

Santopolo, G., Magnusson, J.P., Lindvall, O., Kokaia, Z., and Frisén, J. (2020). Blocking notch-signaling increases neurogenesis in the striatum after stroke. Cells *9*, 8–10.

Slezak, M., Oritz, C.G., Niemiec, A., En, J.F., Chambon, P., Metzger, D., and Pfrieger, F.W. (2007). Transgenic mice for conditional gene manipulation in astroglial cells. Glia *1576*, 1565–1576.

Snippert, H.J., van der Flier, L.G., Sato, T., van Es, J.H., van den Born, M., Kroon-Veenboer, C., Barker, N., Klein, A.M., van Rheenen, J., Simons, B.D., et al. (2010). Intestinal crypt homeostasis results from neutral competition between symmetrically dividing Lgr5 stem cells. Cell *143*, 134–144.

Stange, D.E., Koo, B.-K., Huch, M., Sibbel, G., Basak, O., Lyubimova, A., Kujala, P., Bartfeld, S., Koster, J., Geahlen, J.H., et al. (2013). Differentiated Troy+ chief cells act as reserve stem cells to generate all lineages of the stomach epithelium. Cell *155*, 357–368.

Svensson, V., Natarajan, K.N., Ly, L.H., Miragaia, R.J., Labalette, C., Macaulay, I.C., Cvejic, A., and Teichmann, S.A. (2017). Power analysis of single-cell RNA-sequencing experiments. Nat. Methods *14*, 381–387.

Stuart, T., Butler, A., Hoffman, P., Hafemeister, C., Papalexi, E., Mauck, W.M., Hao, Y., Stoeckius, M., Smibert, P., and Satija, R. (2019). Comprehensive integration of single-cell data. Cell *177*, 1888–1902.e21.

Tamm, C., Böwer, N., and Annerén, C. (2011). Regulation of mouse embryonic stem cell self-renewal by a Yes-YAP-TEAD2 signaling pathway downstream of LIF. J. Cell Sci. *124*, 1136–1144.

Tazaki, A., Tanaka, E.M., and Fei, J.F. (2017). Salamander spinal cord regeneration: the ultimate positive control in vertebrate spinal cord regeneration. Dev. Biol. *432*, 63–71.

Teschendorff, A.E., and Enver, T. (2017). Single-cell entropy for accurate estimation of differentiation potency from a cell's transcriptome. Nat. Commun. *8*, 1–15.

Tirosh, I., Izar, B., Prakadan, S.M., Wadsworth, M.H., Treacy, D., Trombetta, J.J., Rotem, A., Rodman, C., Lian, C., Murphy, G., et al. (2016). Dissecting

the multicellular ecosystem of metastatic melanoma by single-cell RNA-seq. Science *352*, 189–196.

Vanlandewijck, M., He, L., Mäe, M.A., Andrae, J., Ando, K., Del Gaudio, F., Nahar, K., Lebouvier, T., Laviña, B., Gouveia, L., et al. (2018). A molecular atlas of cell types and zonation in the brain vasculature. Nature *554*, 475–480.

Wickham, H. (2016). ggplot2: Elegant Graphics for Data Analysis, Second Edition (Springer).

Zamboni, M., Llorens-Bobadilla, E., Magnusson, J.P., and Frisén, J. (2020). A widespread neurogenic potential of neocortical astrocytes is induced by injury. Cell Stem Cell *27*, 605–617.e5.

Zappia, L., and Oshlack, A. (2018). Clustering trees: a visualization for evaluating clusterings at multiple resolutions. Gigascience *7*, 1–9.

Zeisel, A., Muñoz-Manchado, A.B., Simone, C., Lönnerberg, P., La Manno, G., Juréus, A., Marques, S., Munguba, H., He, L., Betsholtz, C., et al. (2015). Cell types in the mouse cortex and hippocampus revealed by single-cell RNA-seq. Science *347*, 1138–1141.

Zywitza, V., Misios, A., Bunatyan, L., Willnow, T.E., and Rajewsky, N. (2018). Single-cell transcriptomics characterizes cell types in the subventricular zone and uncovers molecular defects impairing adult neurogenesis. Cell Rep *25*, 2457–2469.e8.

STAR★METHODS

KEY RESOURCES TABLE

REAGENT or RESOURCE	SOURCE	IDENTIFIER
Antibodies		
Chicken anti-Nestin	Neuromics	Cat #CH23001,RRID: AB_2148920
Goat anti-Nestin	Neuromics	Cat # GT15114,RRID: AB_2737217
Goat anti-Podocalyxin	R&D	Cat # AF1556,RRID: AB_354858
Goat anti-Sox2	Santa Cruz	Cat # sc-17320, RRID: AB_2286684
Rabbit anti-Sox2	Abcam	Cat # ab97959, RRID: AB_2341193
Goat anti-Sox9	R&D	Cat # AF3075, RRID: AB_2194160
Rabbit anti-Gfap	Dako	Cat # GA524, RRID: AB_2811722
Rabbit anti-Myrf	Gift from M. Wegner	N/A
Mouse anti-O4	Gift from JE. Goldman	N/A
Mouse anti-Tuj1	BioLegend	Cat # 801201, RRID: AB_2313773
Chemicals, peptides, and recombinant proteins		
Tamoxifen	Sigma	Cat # T5648
EdU	Thermo Fisher	Cat # E10415
DAPI	Sigma	Cat # D9542
Critical commercial assays		
Click-iT EdU Alexa Fluor (488, 555 and 647) imaging kit	Thermo Fisher	Cat # C10337 (488), Cat # C10338 (555), Cat # C10340 (647)
RNAscope Multiplex Fluorescent v2 kit	ACDBio	Cat # 323100
Chromium Single Cell 3' Reagent Kit v2	10X Genomics	Cat # PN-120237
Neural Tissue Dissociation Kit	Miltenyi Biotec	Cat # 130-092-628
Deposited data		
scRNaseq (raw data and gene expression matrices)	This paper	GEO: GSE192824
Code for scRNAseq analysis	This paper	https://doi.org/10.5281/zenodo.5851719
Experimental models: Organisms/strains		
Troy-CreERT2 x Rosa26-tdTomato	This paper	N/A
Troy-CreERT2 x Rosa26-Confetti	This paper	N/A
Software and algorithms		
ImageJ	https://imagej.nih.gov/ij/	1.51n
Bitplane Imaris	https://imaris.oxinst.com/	9.1.2
CellRanger	10X Genomics	3.0.1
R	CRAN	3.5.3, 4.0.3
Seurat	Stuart et al., 2019	3.1.4, 4.0.1
Monocle 3	Cao et al., 2019	1.0.0
Python	https://www.python.org	3.9.7
scVelo	Bergen et al., 2020	0.2.4
ggplot2	Wickham, 2016	3.3.2
SCENIC	Aibar et al., 2018	1.1.3
Genie3	Aibar et al., 2018	1.4.3
AUCell	Aibar et al., 2018	1.4.1
RCisTarget	Aibar et al., 2018	1.2.1
LandSCENT	Teschendorff and Enver, 2017	0.99.3
BiomaRt	Durinck et al., 2009	2.38.0
ClusTree	Zappia and Oshlack, 2018	0.4.3

RESOURCE AVAILABILITY

Lead contact

Requests for resources and reagents should be directed to the lead contact, Jonas Frisén (jonas.frisen@ki.se).

Materials availability

Mouse lines and materials used in this study are available upon request.

Data and code availability

- Custom R scripts for single cell RNA sequencing data analysis are deposited at Zenodo. The DOI is listed in the key resources table.
- RNA sequencing data have been deposited at GEO (GEO: GSE192824) and are publicly available at the date of publication. Any additional information required to reanalyze the data reported in this paper is available from the Lead Contact upon request.

EXPERIMENTAL MODEL AND SUBJECT DETAILS

Transgenic mice

Adult (older than 12 weeks) male and female Troy-CreERT2$^{+/-}$ knock-in mice on a Rosa26-tdTomato or Confetti Cre reporter background were used (Slezak et al., 2007; Snippert et al., 2010; Stange et al., 2013).

Mice were housed in groups in standardized cages with a 12:12 h light:dark cycle. They had unrestricted access to food and water. All experimental procedures were performed in accordance with Swedish and European Union guidelines and approved by the institutional ethical board (Stockholms norra djurförsöksetiska nämnd).

Transgenic mouse lines were regularly backcrossed with C57BL/6 mice to ensure fateful expression over time.

METHOD DETAILS

Genetic labeling of transgenic mice

Recombination was induced by 5 daily intraperitoneal injections of 2 mg tamoxifen (20mg/mL in 1:9 ethanol:corn oil) for mice on a Rosa26-tdTomato reporter background or 3 mg for Troy-CreER mice on a Rosa26-Confetti reporter background. Spinal cord injuries were performed after a 1-2 week clearing period following the last tamoxifen injection. For two experiments, injuries were performed 2 and 15 months after tamoxifen injection.

Spinal cord injury

General anesthesia was induced with 4% isoflurane, and maintained with 1.5-2% isoflurane during surgery. Laminectomy was performed at spinal cord segment T9. Following laminectomy, dorsal funiculus incisions were cut transversely across the dorsal funiculus and extended rostrally to span one spinal cord segment using micro surgical scissors (Frisén et al., 1993; Meletis et al., 2008). Full crush lesions were made using Dumont 5 forceps with a 0.1 tip width (Fine Science Tools) without spacers for 2 seconds (Liu et al., 2010). All mice received local anesthesia (Xylocain, AstraZeneca, 10 mg/mL, 2 drops on the spinal cord surface) and analgesia (Carpofen, Pfizer, 5 mg/kg body weight, subcutaneous injection) for pain relief. After crush lesions, an opiate was administered for additional pain relief (Buprenorphine, Actavis, 0.1 mg/kg body weight, subcutaneous injection). An antibiotic was administered daily for the first 3 days after crush lesion (Trimetoprimsulfametoxazol, MSD, 100 mg/kg body weight, subcutaneous injection). Bladders were manually emptied 3 times per day during the first 3 days after crush lesion, and thereafter 2 times per day.

EdU labeling

For analysis of proliferating cells in the uninjured spinal cord EdU (0.75 mg/mL and 1% sucrose) was administrated via the drinking water for 1 week.

For clonal analysis in spinal cord injuries of Troy-CreER mice on Rosa26-Confetti background, EdU was injected intraperitoneally immediately after injury (12.5 mg/mL, 0.1 mL/mouse) followed by EdU administration via drinking water for the remaining 2 weeks of the experiment (0.20 mg/mL and 1% sucrose).

Neural stem cell cultures

To assess the self-renewal and multipotency of Troy-CreER recombined cells *in vitro*, adult mice were administered tamoxifen by daily intraperitoneal injections for 5 days followed by a clearing period of 1 week before initiating neurosphere cultures.

Spinal cord cells were dissociated using papain (Worthington) and neurosphere cultures were established as previously described (Meletis et al., 2008). Prior to dissociation, a small biopsy was taken from the thoracic spinal cord to allow a comparison of *in vivo* and

in vitro recombination rates. Neurospheres were cultured in DMEM/F12 medium supplemented with B27 (2%), bFGF (10 ng/mL) and EGF (10 ng/mL). Primary neurospheres were cultured for ~10-14 days before passaging, and subsequent passages were conducted at an interval of ~5-7 days.

To study self-renewal of Troy-CreER recombined EpA cells compared to other cells in the spinal cord, cultures derived from the Troy-CreER mouse line on a tdTomato reporter background were passaged serially and the recombination rate was recorded before each passage.

In a separate experiment to assess multipotency, single Troy-CreER recombined primary neurospheres were picked manually, dissociated and plated into one well each of an ultra-low attachment 24-well plate (Corning). Clonally derived secondary neurospheres were collected and plated on poly-D-lysine/Laminin (Sigma) coated 96-well plates with DMEM/F12 medium supplemented by 1% FBS (Gibco). After 6-9 days under differentiation conditions, immunocytochemistry was performed.

Immunohistochemistry

Mice were perfused transcardially with PBS followed by 4% formaldehyde in PBS. Spinal cords were post-fixed in 4% formaldehyde in PBS overnight at 4°C, and then cryoprotected in 30% sucrose in PBS. Coronal sections (12 or 20 μm) of thoracic segment ~T9 were collected alternating on slides for all experiments except for the clonal analysis. For the clonal analysis, coronal sections (30 μm) of the injury site at thoracic segment ~T9 were collected serially on slides.

Sections were incubated with blocking solution (10% normal donkey serum and 0.3% Triton-X100 in PBS) for 1 hour at room temperature. Next, sections were incubated with primary antibodies diluted in 10% normal donkey serum overnight. After washing, antibody stainings were revealed using species-specific fluorophore-conjugated secondary antibodies (Cy3, Cy5, Alexa Fluor 488, Alexa Fluor 594, Alexa Fluor 647 or Alexa Fluor 680 from Jackson ImmunoResearch). EdU was detected with the Click-iT EdU Alexa Fluor 488, 555 and 647 imaging kits, using the Manufacturer's instructions. Cell nuclei were visualized with 4',6-diamidino-2-phenylindole (DAPI; 1 mg/mL).

Immunocytochemistry

Cells were incubated with a primary antibody against O4 in DMEM/F12 media with 10% NDS for 60 minutes. After washing off the O4 primary antibody with PBS, cells were fixed in ice-cold 4% formaldehyde in PBS for 15 minutes. After another washing step, Tuj1 and GFAP primary antibodies diluted in 10% normal donkey serum in PBS were left on overnight in 4°C. After washing, the primary antibodies were revealed using species-specific fluorophore-conjugated secondary antibodies (Alexa Fluor 405, Alexa Fluor 488 and Alexa Fluor 647 from Jackson ImmunoResearch).

In situ hybridization with RNAscope

For antigen retrieval, we used target retrieval agent (from ACDBio) for 5 minutes at 95°C. Next, we treated the sections with Protease IV (ACDBio) for 20 minutes at room temperature. The probe (Tnfrsf19, ACDBio) was incubated at 40°C for 2 hours. Next, the probe was revealed using RNAscope Multiplex Fluorescent v2 reagents (ACDBio) and TSA amplification. DAPI was used to reveal cell nuclei. Samples were imaged on a confocal microscope as described below.

Microscopy

Images of tissue sections were acquired using an LSM 700 confocal microscope (Carl Zeiss) or a TCS SP8X confocal microscope (Leica). Images of neurospheres were acquired using an Axiovert 200M inverted microscope (Carl Zeiss), and images of neurosphere differentiation assays were acquired using an inverted LSM 880 confocal microscope (Carl Zeiss). ImageJ 1.51n and Adobe Photoshop CC 2017 were used for image processing.

3D structured illumination microscopy (3D-SIM)

To assess dorsal processes of ependymal cells (see Figures 1A and 1D), 3D-SIM imaging (Gustafsson et al., 2008) was performed using a Plan-apochromat 63X/1.4 NA oil objective on an ELYRA PS.1 microscope (Carl Zeiss). Laser excitation wavelengths were 405 nm, 561 nm and 642 nm, with fluorescence emission detection at 420-480 nm, 570-650 nm, and longpass 655 nm respectively. Raw image stacks (1002x1004 pixels, pixel size 79 nm, 126 nm focus steps) were acquired with 3 rotations and 5 phases. Images were reconstructed using the ZEN 2012 software (Carl Zeiss) with automatic parameter settings. After reconstruction, the SIM images were checked for possible artefacts (e.g. honey comb patterns) to verify appropriate automatic settings. The 3D-SIM system was calibrated using green fluorescent beads (40 nm), yielding a precision of 100±3 nm laterally and 275±8 nm axially.

Single cell RNA sequencing

Troy-CreER mice on a Rosa26-tdTomato background without spinal cord injury (n=4) and with spinal cord injury (n=6, 3 days after dorsal funiculus injury) were sacrificed via decapitation and the spinal cords were collected on ice-cold sterile DPBS supplemented with Glucose, CaCl2, pyruvate and antibiotics (D4031, Sigma). Spinal cords were micro dissected and 5 mm segments centered around the lesion site (or the equivalent regions in uninjured mice) were collected. These were then digested to single cell suspensions using the Neural Tissue Dissociation Kit (Miltenyi) with papain as digestion enzyme. Briefly, tissues were triturated three times in 15-10-10 minute intervals using the GentleMacs Dissociator (Miltenyi) in the presence of papain, and DNAse after the second

trituration. Incubations between trituration were conducted at 37°C under occasional shaking. Cell suspensions were collected in flow cytometry buffer (DPBS supplemented with 10% fetal calf serum), passed through a 70 μm strainer, and myelin debris was partially removed by centrifugation through 0.9M sucrose in DPBS. Cells were resuspended in cytometry buffer and tdTomato expressing cells were sorted into cold DPBS supplemented with 0.04% BSA using an Influx cell sorter (BD) with a 100 μm nozzle. Collected cells were processed for library preparation with the Chromium Single Cell 3' Reagent Kit v2 following the manufacturer's recommendations (10X Genomics). Libraries were sequenced on an Illumina HiSeq 2500 following the recommendations of 10X Genomics.

QUANTIFICATION AND STATISTICAL ANALYSIS

Uninjured tissue

To assess the distribution of recombined ependymal cells, a template was used to divide the ependymal layer into four regions: dorsal, ventral, right, and left (the sum of right and left is presented as lateral in the article) (Figures 1B and S4F and S4G). Recombined and Sox2/Sox9-expressing ependymal cells in each region of the central canal were quantified in 12 μm thoracic coronal sections on randomly selected slides from 14 mice for the EpA subpopulation.

Nestin expression in ependymal cell subpopulations under physiological conditions was assessed by counting Nestin expressing and recombined tdTomato-expressing cells around the central canal. For both subpopulations, Nestin expression was quantified in all ependymal cells of thoracic 12 μm coronal sections on randomly selected slides from 3 mice.

To assess proliferation in ependymal cell subpopulations under physiological conditions, EdU incorporation was quantified in Sox9-expressing unrecombined and recombined cells around the central canal in 12 μm thoracic coronal sections on randomly selected tissue slides from 10 mice for the EpA subpopulation.

To approximate the frequency of Troy-CreER recombined ependymal cells among all cells in a whole tissue section, the number of nuclei labeled by DAPI was automatically counted using the spots function in the Bitplane Imaris software. Counts were made in sections from randomly selected slides containing uninjured thoracic spinal cord from 3 mice. The number of DAPI nuclei in a section was used to determine the percent of recombined ependymal cells among all cells in a spinal cord section, which was estimated to <0.1%.

Neurospheres

The number of recombined and unrecombined neurospheres was quantified in neurosphere cultures from Troy-CreER mice on a Rosa26-tdTomato background (n=4). Quantifications were conducted from the primary neurosphere culture until the 4th passage. To correlate recombination in neurosphere cultures with the *in vivo* recombination of spinal cord ependymal cells, the ratio between Vimentin- and tdTomato-expressing cells around the central canal was quantified in post-fixed biopsies from the spinal cords used for neurosphere cultures.

Injury site quantifications

Injuries in Troy-CreER mice (n=7 dorsal funiculus incisions; n=6 crush lesions) were screened for recombined progeny in the parenchyma. In addition, Troy-CreER dorsal funiculus incision made 2 months (n=3) and 15 months after tamoxifen injection (n=3) were screened for recombined progeny in the parenchyma.

To assess the size of the Troy-CreER ependymal cell population in the injured spinal cord, and its contribution to migrating progeny after 1 week after injury (presented in Figure 2B), Sox2-/Sox9-expressing recombined cells were quantified both around the central canal and in the parenchyma of spinal cord dorsal funiculus incision injury sites. Quantifications were done on randomly selected slides containing 20 μm thick coronal sections from every ~100 μm throughout each lesion area (n=7), where a central canal and migrating progeny could be distinguished, and in corresponding sections from the same region of uninjured control mice (n=6), resulting in 812 recombined Sox2-/Sox9-expressing cells (all recombined and Sox2+/9+ cells were counted in each randomly selected sample). Counts were conducted on whole sections, and normalized to the volume of tissue assessed (number of cells/mm^3 tissue). Out of the recombined Sox2-/Sox9-expressing cells, 338 were assessed for PDGFRß expression. No PDGFRß-expressing cell was found.

To assess the expansion of the Troy-CreER recombined cell population (both ependymal cells and migrated progeny, presented in Figure 2D) after different injury paradigms, Sox2/Sox9 expressing recombined cells were quantified in tissue from dorsal funiculus incisions (n=7 lesion sites), crush injuries (n=6 lesion sites) and in uninjured tissue from the corresponding spinal cord segment (n=6). The maximal population observed in each injury site was then normalized to the average population size in uninjured tissue from the same area of the spinal cord.

To assess Nestin expression in ependymal cells in dorsal funiculus incision injuries, Nestin expressing and recombined cells around the central canal were counted in randomly selected coronal sections spaced ~100 μm apart in and near the injury epicenter (n=3 lesion sites).

Dorsal funiculus incision injuries were screened for both astrocytes expressing Sox9 and oligodendrocytes expressing Sox10 (and NogoA or Myrf) 15 weeks after injury.

Clonal analysis

Serial confocal z-stacks were acquired of 17 injury sites from Troy-CreERT2 mice on a R26-confetti background. The injury site was defined as the area where the surface of the spinal cord was not intact, and/or where migrating progeny leaving the central canal was observed.

The number of ependymal cells recombined to express each fluorescent protein within each lesion site (n=17) was quantified. The frequency of each fluorescent protein was calculated from the same data. Mice with zero recombined Sox2-positive cells in the whole lesion area (n=5 mice) were excluded before further analysis since they would otherwise contribute to a false impression of a lower recombination rate in the mice analyzed downstream.

Instances of recombined ependymal cells appearing in pairs (in the same or adjacent 30 μm sections) was quantified in all serial sections from the imaged lesion sites in order to assess occurrence of symmetric division.

Clones with migrating progeny were identified as recombined Sox2 expressing cells, that had incorporated EdU, and were found outside of the ependymal layer. Recombined ependymal progeny that had left the ependymal layer was quantified in all serial sections from all lesion sites. These quantifications, together with the quantification of all recombination events, were used to determine the proportion of ependymal cells forming clones containing migrating progeny. In this analysis (presented in Figure S4E), one sample with two clones (out of 12 samples with 20 clones containing migrating progeny) was not used as it was not possible to determine the founder cell for each clone with certainty due to a larger number of recombined cells in this sample.

In each clone with migrating progeny, the distances between all cells was measured using ImageJ and Bitplane Imaris. To facilitate measuring the distance between cells in clones with cells in multiple sections, stacks were aligned and merged using Bitplane Imaris.

Single cell RNA sequencing analysis

Sequencing reads were mapped to the mus musculus (mm10) genome with an added tdTomato-WPRE sequence for detection of tdTomato-expression in cells using CellRanger with default parameters. Samples were processed separately and aggregated using Seurat (Stuart et al., 2019), resulting in a dataset that contained ~2,300 cells.

Samples from uninjured and injured spinal cords (3 DPI) were imported into Seurat and merged. Low quality cells were excluded based on expression of few (<500) genes, <1% or >20% mitochondrial reads, or >3 standard deviations more genes expressed compared to the average in the cell population. Doublets were excluded by filtering on co-expression of markers that do not occur in the same cell (i.e. motile cilia marker Foxj1 together with neuronal marker Rbfox3, or endothelial markers Pecam1 and Cldn5). We selected 3000 highly variable genes, and used those for dimensionality reduction with PCA. Based on the Jackstraw plot, we determined that we will use the first 20 principal components for downstream analyses. We next performed UMAP clustering (McInnes et al., 2018). We clustered at different resolutions and used the ClusTree R package to assess clustering performance at different resolutions (Zappia and Oshlack, 2018). A resolution of 0.2 was chosen. 8 clusters were identified, and inspected for tdTomato expression as well as quality readouts including number of unique genes expressed per cell, total gene count per cell, as well as mitochondrial gene expression. The data set contained endothelial cells (EC; n=166), as well as pericytes/fibroblast-like cells (Fib/peri; n=61) (all expressing tdTomato-WPRE, as expected for these cells that are visible in tissue sections). A small cluster of astrocytes (AS; n=35) expressing tdTomato at a lower level compared to ependymal cell populations and perivascular cells was seen. These cells clustered separately from ependymal cells and their progeny, and they were excluded from downstream analyses. Two small clusters of immune cells were identified: microglia (MG; n=66) and lymphocytes (Imm; n=25). Microglia did not express tdTomato, while B lymphocytes expressed tdTomato at a comparable level to the ependymal cells with lowest tdTomato expression. The immune cell clusters were also excluded from downstream analyses. Lastly, the data set contained three clusters of ependymal cells (n=591 + 558 + 437) that expressed tdTomato-WPRE to a comparable extent as the EC and fib/peri clusters, that were also seen in tissue sections. These three clusters were used for downstream analyses.

We identified the 2000 most variable genes among the remaining cells (based on normalized variance, but manually excluding tdTomato-WPRE from the selection), and used those for PCA. Again, based on Jackstraw results, the first 18 components were used for clustering with UMAP. For this clustering, we regressed out the difference between cells in G2M/S phase (using G2M and S phase scores from Seurat's CellCycleScoring function based on the gene list from (Tirosh et al., 2016). Differential expression analysis between clusters was conducted using the non-parametric Wilcoxon Rank Sum test with a threshold of an Bonferroni corrected p value of 0.05 (Table S1).

Monocle 3 was used for cellular trajectory analysis (Cao et al., 2019). Briefly, the variable genes identified in Seurat were used as ordering genes in the Monocle 3 pipeline. Monocle 3 uses a graph embedded algorithm to learn a trajectory that fit the UMAP coordinates. Pseudotime was plotted against other cell qualities using ggplot2 in Figures S7F–S7J (Wickham, 2016).

scVelo was used to calculate RNA velocity in our dataset (Bergen et al., 2020). We first filtered the gene expression matrices to only include the 2,000 most highly variable genes. Then, we computed the moments for velocity estimation using n = 10 nearest neighbors and the top 10 PCs. We calculated the latent time using the cells from the uninjured spinal cord as root. Finally, RNA velocity was estimated based on latent time scores and using the dynamical model.

Signalling entropy was calculated using LandSCENT (Teschendorff and Enver, 2017). LandSCENT contains human protein-protein interaction networks, so we used BiomaRt (Durinck et al., 2009) to convert the mouse gene ID's (MGI symbols) from our data set to the corresponding human gene ID's (HGNC symbol). Mouse gene ID's with more than one corresponding human gene ID's were handled by selecting the top human gene in the list.

Gene regulatory network activity was determined using SCENIC. Direct targets were linked to corresponding transcription factors using the RcisTarget database. The regulon activity for each cell (sum of genes expressed by each regulon) was then assessed using AUCell.

For Figures 4I and 4J, signature/module scores were calculated based on the expression of cluster-specific markers for neural stem cells and transit amplifying cells. Specifically, the lists of genes were obtained after running differential expression analysis among cells from the subventricular zone (Zywitza et al., 2018). We maintained genes specifically expressed in the cell types of interest (i.e., detected in fewer than 20% of cells from all other clusters combined) and used them as input for calculating the signature score using Seurat's AddModuleScore function (genes are listed in Tables S3 and S4).